Natural Hazards
https://doi.org/10.1007/s11069-024-06609-x

ORIGINAL PAPER

Urban flood susceptibility mapping using frequency ratio and multiple decision tree-based machine learning models

Hemal Dey[1,4] · Wanyun Shao[1,2,4] · Hamid Moradkhani[2,3] · Barry D. Keim[5] · Brad G. Peter[6]

Received: 12 November 2023 / Accepted: 3 April 2024

Abstract
Machine learning (ML) models, particularly decision tree (DT)-based algorithms, are being increasingly utilized for flood susceptibility mapping. To evaluate the advantages of DT-based ML models over traditional statistical models on flood susceptibility assessment, a comparative study is needed to systematically compare the performances of DT- based ML models with that of traditional statistical models. New Orleans, which has a long history of flooding and is highly susceptible to flooding, is selected as the test bed. The primary purpose of this study is to compare the performance of multiple DT-based ML models namely DT, Adaptive Boosting (AdaBoost), Gradient Boosting (GdBoost), Extreme Gradient Boosting (XGBoost) and Random Forest (RF) models with a traditional statistical model known as Frequency Ratio (FR) model in New Orleans. This study also aims to identify the main drivers contributing to flooding in New Orleans using the best performing model. Based on the most recent Hurricane Ida-induced flood inventory map and nine crucial flood conditioning factors, the models' accuracies are tested and compared using multiple evaluation metrics. The findings of this study indicate that all DT-based ML models perform better compared to FR. The RF model emerges as the best model (AUC = 0.85) among all DT-based ML models in every evaluation metrics. This study then adopts the RF model to simulate flood susceptibility map (FSM) of New Orleans and compares it with the prediction of FR model. The RF model also demonstrates that low elevation and higher precipitation are the main factors responsible for flooding in New Orleans. Therefore, this comparative approach offers a significant understanding about the advantages of advanced ML models over traditional statistical models in local flood susceptibility assessment.

Keywords Flood susceptibility mapping · Machine learning · Random forest · Frequency ratio · New Orleans

1 Introduction

Climate change is expected to intensify the frequency and severity of hydrological extremes such as flooding (Held and Soden 2006). From 2000 to 2018, a total of 2.23 million km^2 area has been flooded around the world, consequently 255–290 million

Extended author information available on the last page of the article

people were directly affected (Tellman et al. 2021). Climate change is also expected to continue to drive substantial sea level rise throughout the twenty-first century (Sweet et al. 2022; Kopp et al. 2017). Coastal cities around the world are thus under enormous stress from climate change-driven events and long-term changes coupled with increasing population and infrastructure concentrations (Brown et al. 2019; Wong et al. 2014; USGCRP 2018). In the United States (U.S.), with 280 million urban population, urban flooding can lead to immense social and economic damages (NAS 2019). For example, in 2005, the state of Louisiana witnessed devastating flood damages induced by Hurricane Katrina resulting in around 1,067 reported fatalities. This disaster left 283,838 houses fully destroyed, 73,172 with sustained major damages, and 69,763 with minor damages (FEMA 2006). Notably, in New Orleans, the flood damages to the residential properties are estimated in a total of $16 billion, while damages to the public structure and utilities such as roads, railroads, drainage, water defense and electricity network, totaled in $7 billion (Pistrika and Jonkman 2010). Meanwhile, the risk of coastal flooding is projected to increase in the near future (Hallegatee et al. 2013). To ensure effective mitigation, it is imperative to identify the highly susceptible regions through the best quantitative method so that the limited resources can be concentrated at these areas.

A substantial amount of research has already been conducted on flood hazard mapping using a variety of geospatial techniques (e.g., Dano et al. 2019; Das 2020; Hoque et al. 2019; Khosravi et al. 2016; Rahman et al. 2021; Samanta et al. 2018; Sarkar and Mondal 2020; Shahabi et al. 2020; Tehrany et al. 2014, 2015a; Tehrany and Kumar 2018) and hydraulic modeling (HEC-RAS) (Elkhrachy et al. 2021). Among all these geospatial techniques based bivariate statistical models such as, Shannon's entropy, Weighting factor, Statistical index (Khosravi et al. 2016) and Frequency Ratio (FR), the FR model is a widely used bivariate statistical model, establishing relationships between flood locations and the classes of different flood conditioning layers (Samanta et al. 2018; Sarkar and Mondal 2020; Tehrany et al. 2015a; Rahmati et al. 2016). But FR is deemed a conventional method for mapping flood susceptibility due to its simple formula and straightforward process, albeit time-consuming and laborious (Sahana et al. 2020). Due to the rapid progress in machine learning (ML) and computation power, the FR model has become less ideal over time (Wang et al. 2020b). To date, an increasing number of researchers use more sophisticated empirical ML modelss to assess natural hazards risks. Some common algorithms include Decision Tree (DT) (Khosravi et al. 2018), Multivariate Logistic Regression (MLR) (Rahman et al. 2019; Tehrany et al. 2014), CART (classification and regression trees) (Abedi et al. 2022; Rahman et al. 2021), Support Vector Machine (SVM) (Sahana et al. 2020; Tehrany et al. 2015a), Random Forest (RF) (Farhadi and Najafzadeh 2021; Lee et al. 2017), Adaptive Boosting (AdaBoost) (Al-Abadi 2018), Gradient Boosting (GdBoost) (Costache et al. 2020), Extreme gradient boosting (XGBoost) (Abedi et al. 2022), Artificial Neural Network (ANN) (Falah et al. 2019; Rahman et al. 2019), Deep Learning (DL) (Shahabi et al. 2021), Convolutional Neural Network (CNN) (Wang et al. 2020a). Among them, DT-based algorithms especially RF is considered as the standard machine learning algorithm for modeling flood susceptibility (Islam et al. 2021). The RF model offers numerous advantages over the other ML models for classification, including the ability to handle missing data and outliers, less susceptible to overfitting, capability of producing more accurate results by handling large volumes of datasets (Elmahdy et al. 2020; Géron 2022; Lee et al. 2017; Rodrigues and De la Riva 2014). Researchers have

applied both FR and DT-based ML models in a number of natural hazards susceptibility mapping studies and concluded DT-based ML models such as RF can perform better than FR by predicting more accurately.

In a study by Wang et al. (2020b), the performances of the FR and RF models for landslide susceptibility mapping were compared in Yunyang County, China, and it was found that the RF performed better compared to FR. Elmahdy et al. (2020) used RF and FR model to map land subsidence and sinkholes susceptibility in Al Ain area, UAE. RF was found to be highly accurate and required less time to generate results. Furthermore, Amare et al. (2021) adopted FR and RF models to assess the susceptibility of gully erosion in Ethiopia and found the accuracy of FR varies between good to average while the RF model achieved excellent accuracy. Han et al. (2020) examined the prediction accuracy of FR, DT and RF models for seismic vulnerability assessment in South Korea and revealed that the RF showed the highest accuracy. Thanh et al. (2022) mapped the groundwater potential zone in Kanchanaburi Province of Thailand using FR, RF and AHP and compared their performances. They found the best performance from RF model. Some of the studies also found that RF outperformed other statistical models such as Logistic Regression and Bayes discriminant analysis for debris flow susceptibility mapping in Nyalam County, Tibet (Liang et al. 2020).

Despite a large number of studies using different machine learning models to map various hazards susceptibilities, there however has been little research that explicitly compares the performances of DT-based ML models with the FR model for flood susceptibility mapping by considering multiple evaluation metrics. The main goal of this study is to address this knowledge gap. Thus, it aims to not only compare the accuracy of FR with that of multiple DT-based ML models in flood susceptibility but also identify the best performing ML model and its benefits.

To do so, New Orleans, Louisiana in the United States is selected as the study area. New Orleans has experienced several high-impact floods historically and has received wide attention due to its enormous damages and losses to floods, especially during and since Hurricane Katrina (Keim and Muller 2009). Its geographic location that is largely below sea level, along with its vulnerable population, renders New Orleans highly susceptible to flooding (Cai et al. 2016; Elliott and Pais 2006). Specifically, the primary rationale for selecting New Orleans is three-fold. First, Keim and Muller (1992 and 1993) show that heavy rainfall has been historically a problem for the city, but particularly since the May 3rd flood of 1978. Since then, numerous heavy rainfalls have flooded the city. A recent example is the event that occurred on July 10, 2019, when an upper-level trough associated with Hurricane Barry produced 100–200 mm of rain in 3 h, thereby flooding much of the French Quarter, Central Business District, and Uptown New Orleans (National Centers for Environmental Information 2019). Furthermore, Brown et al. (2019) demonstrated that rainfalls all across the Southeast, including in New Orleans, are becoming shorter in duration and more intense over time, leading to more flash floods. Second, coastal Louisiana, in which New Orleans is located, is projected to have high flood risk in the next 30 years (Wing et al. 2022) and is among the most vulnerable locations in the world as it pertains to climate change. Third, New Orleans has a long history of social inequality and racial injustice, largely contributing to the disproportionately devastating impacts of and longer recovery from Hurricane Katrina among the socially vulnerable populations such as African Americans, people living in poverty, and the less educated (Finch et al. 2010). Hence, using New Orleans as a case study can provide critical lessons learned for coastal cities around the world.

2 Data and methods

2.1 Datasets and sources

Multiple datasets were required in this study to conduct the comparative analysis of model performance and delineate flood susceptibility zones. A brief description of each dataset and its source, along with their output, is displayed in Table 1. The process of producing flood susceptibility maps is laid out in Fig. 1. Each of the following subsections specifically discusses each component.

2.2 Method

Flood susceptibility analysis can be divided into three major steps. These are: (1) producing the flood inventory map; (2). preparing thematic layers of all flood conditioning factors (FCFs); (3) evaluating the model's accuracy with multiple metrics and (4) flood susceptibility mapping.

2.2.1 Flood inventory map

A flood inventory map displays past locations of floods in a specific region, based on historical flood events. In the flood susceptibility analysis, the flood inventory map is considered the most essential element. According to Manandhar (2010), scientifically justified data of historical flood events are critical to identify flood susceptibility zones and predict future flood locations. Furthermore, the flood inventory map helps to identify relationships among FCFs (Rahman et al. 2021). In this study, a recent 2021 flood event in New Orleans induced by Hurricane Ida that struck coastal Louisiana on 29th August, 2021 (Beven et al. 2022; Omer 2021) was considered to produce the flood inventory map. The entire process of developing a flood inventory map was conducted on the Google Earth Engine (GEE; Gorelick et al. 2017) platform using JavaScript API. Sentinel-1 SAR (Synthetic Aperture Radar) data have been used to extract flooded zones because of its fine spatial resolution (10 m) and cloud-penetrating quality. Atmospheric correction (spatial filtering) was required to reduce the 'salt and pepper' noise of the Sentinel-1 SAR raw imagery. To extract the flooded zone, several Sentinel-1 SAR images comprising pre-flood and post-flood period were considered in this study. These pre-flood images were combined together and post-flood images were combined as well to obtain more precise surface water data. A division band ratio algorithm was then applied to both stacked images to extract the total inundated area. Water pixels that appeared in both images (pre-flood and post-flood) were considered permanent water bodies. Pixels that appeared as water bodies in post-flood images but did not show in pre-flood images were deemed as flood pixels (Islam and Sado 2000). In addition, to identify more precise flooded zones, the Global Surface Water dataset by Pekel et al. (2016) was masked out from the total inundated area. A total of 200 inventory points were selected randomly, consisting of 100 points from flooded zones and 100 points from areas outside the flooded zones. Flooded points were labeled as 1 while non-flooded points were labeled as 0. Based on previous research (Samanta et al. 2018; Sarkar and Mondal 2020), 70% of flood pixels were randomly selected from the flood

Table 1 Datasets and sources used in this study

Dataset	Data source	Temporal range	Spatial resolution (m)	Mapping output
Sentinel-1 SAR GRD	ESA/Copernicus	2021	10	Flood inventory map
JRC/GSW1_2/Global Surface Water	Pekel et al. (2016)	2020	30	Flood inventory map
OREGONSTATE/PRISM/ Norm91m	PRISM/OREGON STATE	1991–2020	928	Precipitation
USGS/3DEP/10 m	USGS	–	10	Elevation, Slope, Aspect, TWI, Drainage density
Open Land Map Soil Texture Class	Hengl. (2018)	2018	250	Soil Texture
Sentinel-2 MSI	ESA/Copernicus	2021	10	LULC
Landsat-8 OLI/TIRS	USGS	2021	30	NDVI

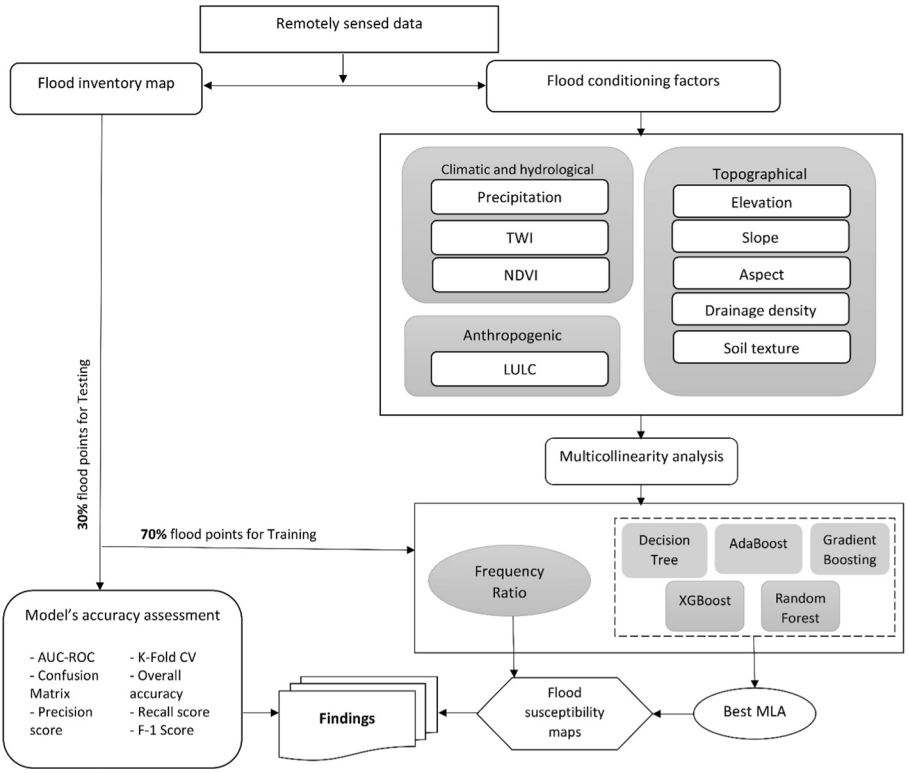

Fig. 1 Conceptual and methodological framework

inventory points as training data, and the remaining 30% flood points were used as testing data for validation.

The flood inventory map reveals that the potential flooded area due to Hurricane Ida is about 10.8 km^2 in New Orleans (Fig. 2). Most flooding points were found to be in the proximity of Lake Saint Catherine and some flood pixels were detected inside the downtown area alongside the Mississippi River.

2.2.2 Flood conditioning factors (FCFs)

Flood conditioning factors refer to variables that have direct or indirect influences on flood occurrences. To map the flood susceptibility zones, it is essential to identify relevant FCFs and to categorize their impacts on flood occurrences (Kia et al. 2012). Therefore, based on an extensive literature review (e.g. Dano et al. 2019; Das 2020; Hoque et al. 2019; Kia et al. 2012; Rahman et al. 2019, 2021; Rahmati et al. 2016; Samanta et al. 2018; Sarkar and Mondal 2020), a total of nine conditioning factors of flooding from several domains (e.g., topographical, anthropogenic, climatic, and hydrological) were selected. Later, a multicollinearity analysis using Pearson correlation was conducted among the nine factors to check if there were any severe correlations existing among them. The findings from Pearson's correlation analysis demonstrate that no correlation values were found above 0.80, suggesting the absence of multicollinearity among the FCFs (Fig. 3).

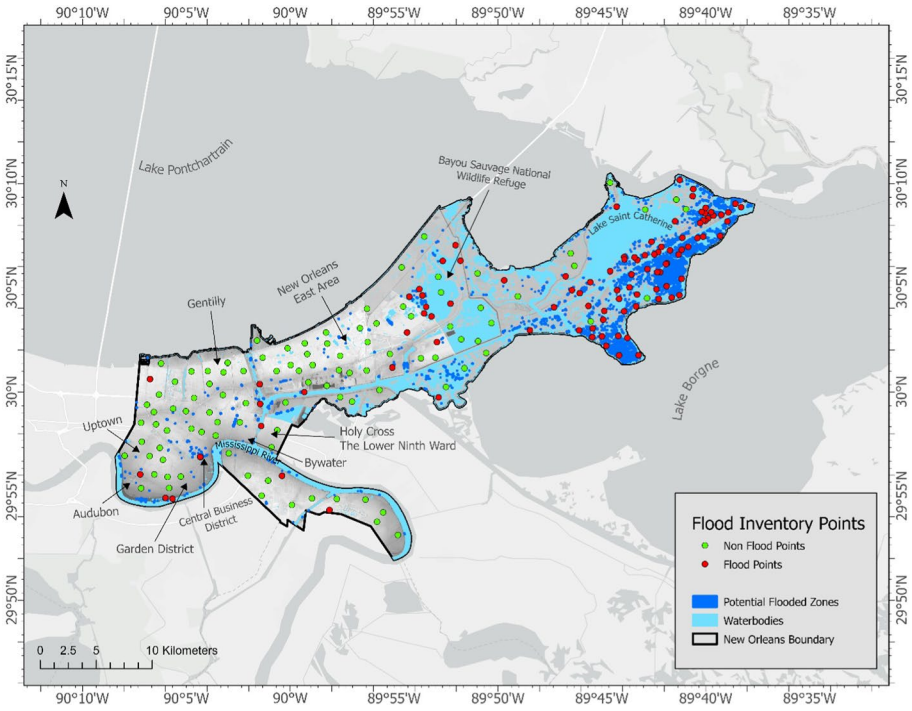

Fig. 2 Flood inventory map of 2021 Hurricane Ida induced flood in New Orleans. Blue color represents the potential flooded areas, Cyan color represents the waterbodies, Red points represents flood points and Green points represents non-flood points

Following multicollinearity analysis, nine FCFs including elevation, slope, aspect, precipitation, land use land cover (LULC), normalized difference vegetation index (NDVI), drainage density, topographic wetness index (TWI) and soil texture layers are collected from different sources (Table 1). A brief description of each FCFs is given on Table 2 with their Max-Min value or classes for New Orleans.

Since these FCFs had different spatial resolution and geographic coordinate system (GCS), The layers with coarse resolutions were resampled into 10 m and converted into GCS NAD 1983 using ArcGIS Pro 2.8 software to match their spatial scale and GCS with others.

Figure 4 displays the spatial distribution of each FCF across New Orleans. A vast area in New Orleans has a low elevation, even below sea level within levee protection (Fig. 4a), low slope (Fig. 4b), and flat aspect (Fig. 4c) rendering it at high risk of flooding. Relatively high elevations are found adjacent to the Mississippi River, which comprise the natural levee of the river. Artificial levees are erected on top of the natural levees to protect the city from river flooding. With 112.40 km^2 of urban land, 223.72 km^2 of forest land, 86.82 km^2 of grassland, 57.81 km^2 of barren land, and 142.19 km^2 of water bodies, New Orleans city historically grew outward from the hub in the western part which includes Downtown and historic French Quarter (Fig. 4e). Precipitation tends to be slightly concentrated in the south and eastern part of New Orleans (Fig. 4d). TWI values are high in the New Orleans east area and especially along elongated water bodies such as the lake Saint Catherine and

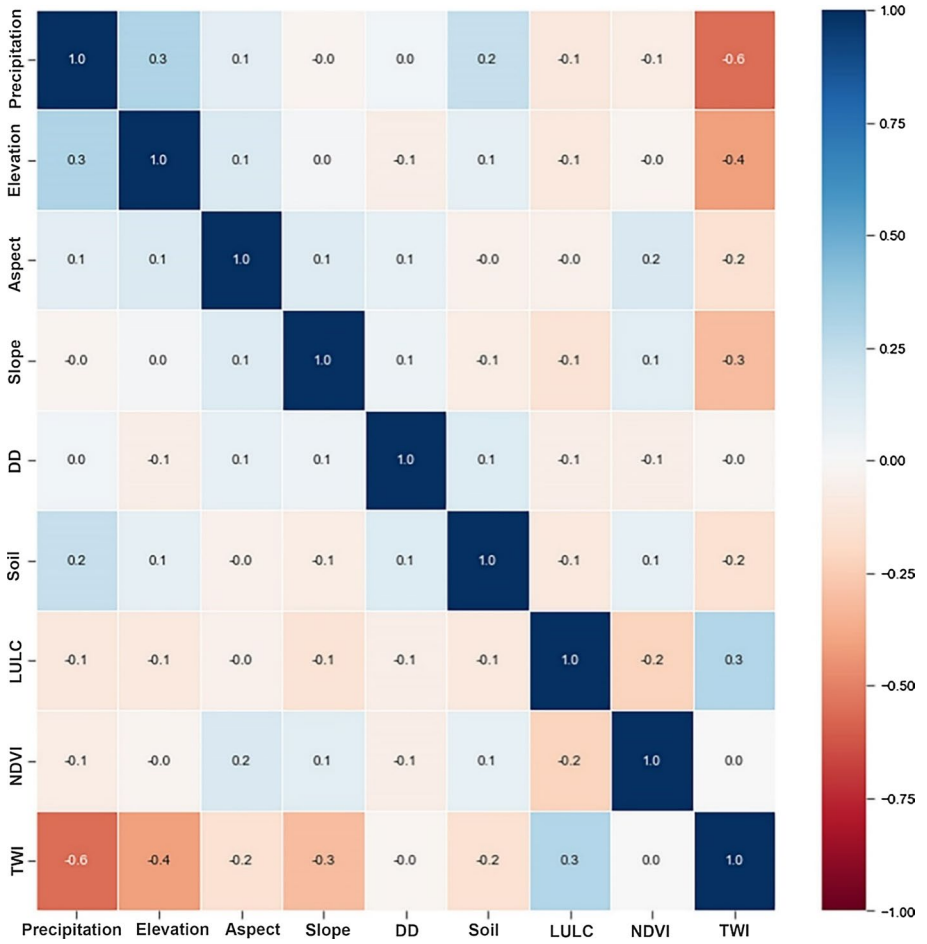

Fig. 3 Multicollinearity analysis via Pearson correlation matrix among flood conditioning factors

Mississippi River (Fig. 4h). Meanwhile, the drainage density tends to be higher across the urban areas and along water bodies in the western part of New Orleans because of the bowl shape, low elevations, and lack of topographic relief. In addition, most of New Orleans is covered with clay loam (ClLo) and sand clay loam (SaClLo) soil (Fig. 4i). SaClLo soil texture is considered highly susceptible to flooding (Rahmati et al. 2016). The NDVI values are high along the Mississippi River are relatively high within vegetated parts of the urban areas (Fig. 4f) as well.

2.2.3 Adopted models for flood susceptibility mapping

2.2.3.1 Frequency ratio FR model, a traditional statistical method, was first adopted to prepare the flood susceptibility map (FSM) of New Orleans. The FR critically analyzes the contribution of each class of each FCF on potential future flooding (Lee et al. 2012; Rahmati et al. 2016; Samanta et al. 2018; Sarkar and Mondal 2020).

Table 2 Flood conditioning factors and their association with flooding

Factor	Association of FCFs with flood susceptibility	Value range / Classes	References
Elevation	Elevation is a significant factor in flood susceptibility as gravitational force drives surface runoff to flow from higher to lower altitude and consequently water accumulates on flat or bowl-shaped regions	Max: 19.65 m Min: −7.87 m	Sarkar and Mondal (2020)
Slope	Slope controls the velocity of surface runoff, flood water accumulation process, and infiltrated water amount. The regions with low slope and flat topography are more susceptible to flooding	Max: 31.18° Min: 0°	Das (2020)
Aspect	Aspect influences the precipitation patterns and surface water runoff as it refers to the specific direction of land surface. It also helps to assess the water flow direction	flat, north (0°-22.5°), northeast, east, southeast, south, southwest, west, northwest, and north (337.5°–360°)	Tehrany and Kumar (2018)
Precipitation	Precipitation is positively correlated with flood occurrences resulting in waterlogging and flooding. Heavy precipitation significantly increases the probability of flooding in a particular region	Max: 141.65 mm Min: 133.98 mm	Ali et al. (2019), Hoque et al. (2019)
LULC	LULC influences flood occurrence as inefficiently planned urbanization and concrete surface would increase flood susceptibility while vegetation cover reduces flood susceptibility by preventing rapid runoff and aiding infiltration	Urban land, Forest land, Grassland, Barren land, Waterbodies	Tripathi et al. (2014)
NDVI	NDVI is an important factor determining flood susceptibility as dense vegetation hinders surface water flow and stimulates infiltration. Therefore, a region with denser vegetation (NDVI value > 0.4) has lower flood susceptibility. NDVI was calculated using following Eq. 1, NDVI = (NIR-Red)/(NIR + Red) (1) In Eq. 1, Red and NIR represent the Red band and Near Infrared band of Landsat 8 images respectively	Max: 0.85 Min: −0.58	Paul et al. (2019), Quader et al. (2021)

Table 2 (continued)

Factor	Association of FCFs with flood susceptibility	Value range / Classes	References
Drainage density	Drainage Density is defined as the ratio of the total length of channel segment to the basin area, influences both peak discharge and water flow direction. Higher drainage density indicates a higher probability of flooding	Max: 983.07 km^2 Min: 0 km^2	Ogden et al. (2011)
TWI	TWI is an index used to estimate the tendency of water to accumulate in any area within a watershed. A higher TWI value indicates a higher susceptibility of flooding. The following formula (Eq. 2) used to calculate TWI, $TWI = In(A_S / \tan \beta)$ (2) where, A_s is the specific catchment area (in m^2/m) and β is the slope (in radians)	Max: 88.38 Min: −8.81	Shahabi et al. (2020)
Soil texture	Soil Texture is a vital factor that influences floods because the total rate of surface runoff, infiltration, and percolation depend on the soil textures of that area to a large extent	Cl, SaCl, ClLo, SiClLo, SaClLo, Lo, SiLo, SaLo	Rahmati et al. (2016), Rahman et al. (2021)

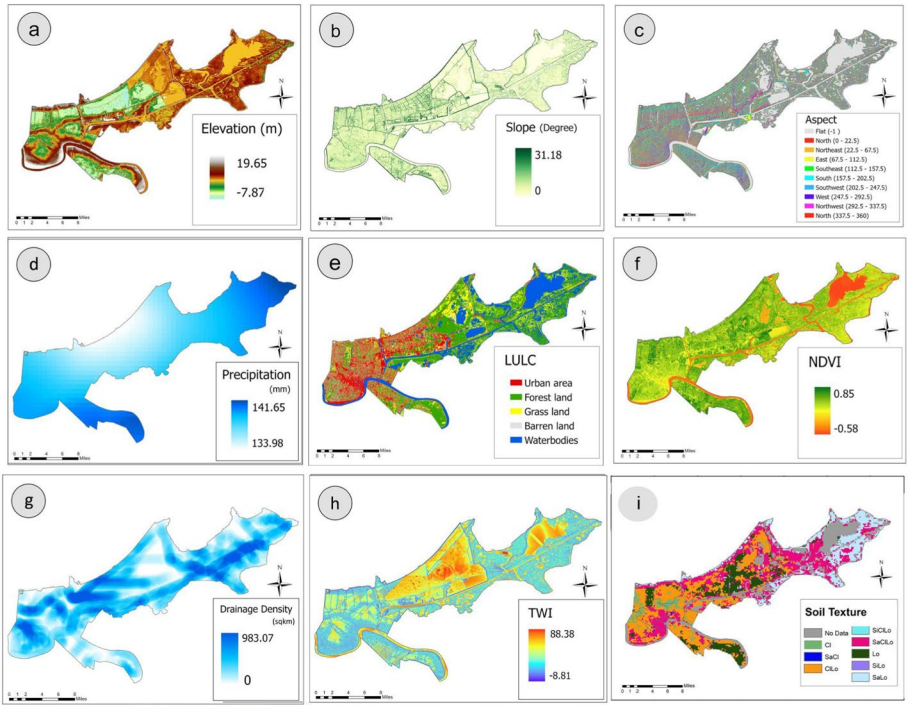

Fig. 4 Thematic layers of flood conditioning factor used in flood susceptibility mapping. **a** Elevation, **b** Slope, **c** Aspect, **d** Precipitation, **e** LULC, **f** NDVI, **g** Drainage density, **h** TWI, and **i** Soil texture

To conduct FR analysis, it was necessary to reclassify all the thematic layers of factors into several classes (Table 3). The Natural breaks classification method by Jenks (1967) was used in several layers based on their class types and values.

Later, 70% flood pixels from the flood inventory map were used to train the FR model. The FR values were measured by calculating the ratio of percentages of flood pixels for each class to the percentage of total pixels for that particular class (Tehrany and Kumar 2018). The FR values for each class of every flood conditioning factor was calculated using the following Eq. 3:

$$\mathrm{FRi} = \frac{\mathrm{Fpixi} / \sum_{i=1}^{n} F\mathrm{pixi}}{Tpixi / \sum_{i=1}^{n} T\mathrm{pixi}} \tag{3}$$

where $\mathrm{FR_i}$ is the frequency ratio value for class i of each factor variable. $F\mathrm{pix_i}$ represents the number of flood pixels for i class and $T\mathrm{pix_i}$ represents the total number of actual pixels of that i class. n represents the total number of classes for each FCF. After calculating the $\mathrm{FR_i}$ values, they were summed up to calculate flood susceptibility index (FSI). The formula of FSI-FR is given below on Eq. 4:

$$\mathrm{FSI-FR} = \sum_{j=1}^{n} FRi \tag{4}$$

Table 3 The FR model results for each class of flood conditioning factors

Flood conditioning factor	Class	Total pixels number	% of total pixel	Flood points	% of flood points	FR
Elevation	− 7.88–1.18	973,627	15.60	3	4.29	0.27
	− 1.18–0.11	2,761,484	44.23	14	20.00	0.45
	0.11–1.41	2,058,037	32.97	52	74.29	2.25
	1.41–4.42	392,800	6.29	1	1.43	0.23
	4.42–19.65	57,033	0.91	1	1.43	1.56
Slope	0–0.61	4,215,157	67.83	54	77.14	1.14
	0.61–1.95	1,516,766	24.41	14	20.00	0.82
	1.95–4.27	336,299	5.41	2	2.86	0.53
	4.27–8.19	113,642	1.83	0	0.00	0.00
	8.19–31.18	32,263	0.52	0	0.00	0.00
Aspect	Flat	356,068	21.08	2	2.86	0.14
	North	326,807	5.23	4	5.71	1.09
	Northeast	575,023	9.21	11	15.71	1.71
	East	595,301	9.54	4	5.71	0.60
	Southeast	602,371	9.65	5	7.14	0.74
	South	677,434	10.85	12	17.14	1.58
	Southwest	576,269	9.23	10	14.29	1.55
	West	604,075	9.68	8	11.43	1.18
	Northwest	1,315,908	9.83	7	10.00	1.02
	North	613,725	5.70	8	11.43	2.00
Precipitation	133.98–135.72	917,427	14.69	4	5.71	0.39
	135.72–137.11	1,178,965	18.88	7	10.00	0.53
	137.11–138.43	1,283,923	20.56	4	5.71	0.28
	138.43–139.75	1,684,899	26.99	26	37.14	1.38
	139.75–141.64	1,178,122	18.87	29	41.43	2.20

Table 3 (continued)

Flood conditioning factor	Class	Total pixels number	% of total pixel	Flood points	% of flood points	FR
LULC	Urban land	1,124,935	18.02	6	8.57	0.48
	Forest land	2,238,636	35.86	47	67.14	1.87
	Grassland	869,408	13.93	12	17.14	1.23
	Barren land	577,967	9.26	2	2.86	0.31
	Waterbodies	1,432,386	22.94	4	5.71	0.25
NDVI	−0.58–0.38	817,995	13.10	1	1.43	0.11
	−0.38–0.03	314,703	5.04	1	1.43	0.28
	0.03–0.31	1,110,506	17.79	18	25.71	1.45
	0.31– -0.56	2,497,785	40.01	48	68.57	1.71
	0.56–0.89	1,502,347	24.06	3	4.29	0.18
Drainage density	0–96.37	1,781,170	28.74	14	20.00	0.70
	96.37–212.03	1,860,087	30.02	20	28.57	0.95
	212.03–350.82	1,592,906	25.71	18	25.71	1.00
	350.82–547.43	804,391	12.98	13	18.57	1.43
	547.43–983.07	157,927	2.55	4	5.71	2.24
TWI	−8.81–2.71	2,330,905	37.51	47	67.14	1.79
	−2.71–0.71	2,028,396	32.64	30	18.57	0.57
	0.71–22.44	1,854,384	29.84	10	14.29	0.48
	22.44–55.61	413	0.01	0	0.00	0.00
	55.61–88.38	27	0.00	0	0.00	0.00

Table 3 (continued)

Flood conditioning factor	Class	Total pixels number	% of total pixel	Flood points	% of flood points	FR
Soil texture	CI	198,960	3.94	1	1.43	0.36
	SaCI	14,999	0.30	0	0.00	0.00
	CILo	1,694,924	33.59	9	12.86	0.38
	SiCILo	506	0.01	0	0.00	0.00
	SaCILo	1,666,650	33.03	19	27.14	0.82
	Lo	712,958	14.13	2	2.86	0.20
	SiLo	1680	0.03	0	0.00	0.00
	SaLo	755,409	14.97	31	44.29	2.96

where *j* is each FCF considered in this study and n is the total number of FCFs. Later, natural breaks were used for reclassification after summing up the FSI-FR because it is considered the most suitable when there are big 'leaps' in the data (Ayalew and Yamagishi 2005). FSI-FR values were accordingly classified into five major categories (i.e., very low, low, moderate, high, and very high). The entire process of FSI-FR calculation was conducted using ArcGIS Pro 2.8 software.

2.2.4 Multiple decision tree-based algorithms

In this study, five decision tree-based (DT-based) ML model were adopted such as DT, AdaBoost, GDBoost, XGBoost, and RF. These DT-based ML models were run with their default parameter on the Jupyter Notebook using Python language. A brief description of each DT-based ML models is provided below.

2.2.5 Decision tree

DT is a versatile ML model that can effectively solve classification, regression, and multi-output tasks, as well as can handle complex datasets (Géron 2022). It is a widely used ML model due to its simplicity. This model has a tree-like structure that splits data into different branches depending on input feature. Each DT includes root nodes, child nodes, and leaf nodes where the final predictions come from the leaf nodes (Han et al. 2020). Additionally, it offers several benefits such as the ability to handle large multi-dimensional datasets, the ability to identify homogenous clusters with various susceptibility levels and ability to predict outcomes by detecting complex feature relationships (Tehrany et al. 2013). In this study, DT model was conducted by importing *DecisionTreeClassifier* from SciKit Learn package (Pedregosa et al. 2011).

2.2.6 Adaptive boosting

Adaptive Boosting, also known as Adaboost, is an ensemble ML model that combines several weak learners into a strong learner with each new predictor by paying more attention to fixing the mistakes of its predecessor (Géron 2022; Madhuri et al. 2021). Initially a subset from the training set and a classifier-based tree (e.g., a DT) is built, assuming equal weight for all instances in AdaBoost model. Then, the model predicts instances and adjust relative weight of misclassified ones while keeping the weight unchanged of correctly classified instance during each iteration. Next, the weight of all the instances is normalized and a new subset is formed through random sampling to build the next classifier-based model. This iterative process continues until it meets terminated conditions (Al-Abadi 2018; Tien Bui et al. 2016). Through this process a weak learner turns into a strong learner by gradually making it better. In this study, the Adaboost algorithm was applied using *AdaBoostClassifier* from SciKit Learn package (Pedregosa et al. 2011).

2.2.7 Gradient boosting (GdBoost)

GdBoost is a ML model that sequentially add predictors to an ensemble of DT where each tree fixed the errors made by its previous one (Géron 2022). It incorporates gradient descent optimization to fit the trees by minimizing loss function and recalibrating the weight of training samples in each iteration. This model is capable of effectively solving

classification problems if the target variables are categorical and regression problems if the target variables are continuous, while also handling complicated nonlinear relationship between input feature and output variables (Costache et al. 2020). These attribute makes this model more suitable for flood forecasting based on multiple FCFs (Ghanim et al. 2023). The *GradientBoostingClassifier* was imported from SciKit Learn package (Pedregosa et al. 2011) to conduct the GdBoost classification.

2.2.8 Extreme gradient boosting (XGboost)

XGboost is a scalable tree boosting ML model that is specifically created to achieve fast and high performance (Hasanuzzaman et al. 2022). XGBoost differs from other methods by generating a series of sequential decision trees, instead of averaging independent trees. Each tree is built using the prediction errors or residuals of the previous tree model (Abedi et al. 2022). It utilizes tree pruning with many tunable parameters which helps to prevents overfitting, handle missing data and improve overall prediction accuracy (Hasanuzzaman et al. 2022; Madhuri et al. 2021). This study imported *XGBClassifier* from xgboost module to predict flood susceptibility.

2.2.9 Random Forest (RF)

RF is one of the most powerful ensemble ML model introduced by Breiman (2001). The RF algorithm is a versatile algorithm that can be used to solve a wide range of classification and regression tasks (Géron 2022). RF employs bagging method, also known as bootstrap aggregating sampling, to selects subsets randomly from the training set and constructs multiple decision trees for all of them. Bootstrapping sampling is the sampling method of selecting a random subset with replacement from a total dataset. For each bootstrap sample, one decision tree is grown by recurrently splitting the data based on the best split that has less impurity (Elmahdy et al. 2020). Each decision tree in the RF generates a prediction at its leaf nodes (Farhadi and Najafzadeh 2021).The final prediction is determined by the majority votes (for classification) or average votes (for regression) found from all decision trees (Géron 2022; Lee et al. 2017). RF offer several advantages such as enhanced accuracy, ability to reveal features importance, ability to avoid overfitting, ability to handle large and high dimensional data, ability to effectively deal with missing values and outliers inside the predictor variables (Amare et al. 2021; Elmahdy et al. 2020; Farhadi and Najafzadeh 2021; Youssef et al. 2022). Most importantly each feature can act as the predictor during the segmentation process in RF (Wang et al. 2020c).

In this study, the RF classifier was run by importing *RandomForestClassifier* from SciKit Learn package (Pedregosa et al. 2011). Later, the *feature_importances* function was utilized to reveal the importance of different FCFs on flood occurrence in New Orleans city. To generate FSM, the probability of flood occurrence was simulated using *predict_proba* function that creates flood susceptibility index (FSI) for each pixel. FSI-RF model is range between 0 and 1, where 0 indicates nonprobability of flooding and 1 indicates probability of flooding. Hence, the pixels with a values closer to 1 are very high flood susceptible while the pixels with a value closer to 0 are very low flood susceptible. Therefore, the equal interval method was chosen to categorize FSI-RF into five distinct classes, namely very low (0–0.2), low (0.2–0.4), moderate (0.4–0.6), high (0.6–0.8), and very high (0.8–1.0) susceptibility using ArcGIS Pro 2.8.

This study also utilized 2022 US census data and calculated the exposed populations residing in high flood prone areas classified by FR and RF model.

2.2.10 Accuracy assessment of FR and multiple DT-based ML models

In this study, the receiver operating characteristic (ROC) curve was considered to compare the performance of FR model with that of multiple DT-based ML models in flood susceptibility mapping. The ROC curve is a universal scientific method to assess the accuracy level of any prediction models because of its accessible and transparent way of indicating accuracy (Sarkar and Mondal 2020; Tehrany et al. 2013).

The process of validation for FR model was implemented using testing flood pixels data and predicted FSM in ROC tool of ArcSDM toolbox. The process of ROC-AUC for the multiple DT-based ML models was conducted using *plot_roc_curve* tools from the SciKit learn package (Pedregosa et al. 2011) on Python.

The X axis of the ROC curve represents false positive rate (FPR) (1- specificity) (Eq. 5) and the y axis represents true positive rates (TPR) (sensitivity) (Eq. 6). Where, TP = true positive; FP = false positive; TN = true negative; FN = false negative.

$$\text{X axis} = \text{FPR}\,(1 - \text{specificity}) = 1 - \left[\frac{TN}{TN + FP}\right] \tag{5}$$

$$\text{Y axis} = \text{TPR}\,(\text{sensitivity}) = \left[\frac{TP}{TP + FN}\right] \tag{6}$$

This research also conducted multiple accuracy assessments including confusion matrix, K-Fold cross validation, overall accuracy, precision score, recall and F-1 score, to identify the optimal model among DT-based ML models. K-Fold cross validation is a technique to evaluate ML models, especially when dealing with limited data samples (Madhuri et al. 2021). K-fold cross validation process is the best to way validate limited data by dividing itself into K equally sized subsets where one subset is used as a testing set and the rest of K-1 subsets are used as training sets. This study adopted 5-Fold cross validation to identify the best model among DT-based ML models. The overall accuracy calculates the total correct prediction of flood and non-flood pixels, precision score quantifies the ratio of classified flood pixels and actual flood pixels, recall scores assess only correctly classified flood pixels among all correctly classified pixel and F-1 score is the harmonic average of precision and recall score (Han et al. 2020). The formula to assess overall accuracy, precision score, recall score and F-1 score are given on Eqs. 7–10 respectively.

$$\text{Overallaccuracy} = \frac{TP + TN}{TP + FP + TN + FN} \tag{7}$$

$$\text{Precisionscore} = \frac{TP}{TP + FP} \tag{8}$$

$$\text{Recallscore} = \frac{TP}{TP + FN} \tag{9}$$

$$\mathrm{F}-1\ \mathrm{score}\ = \frac{(2 \times Precision \times Recall)}{(Precision + Recall)} \tag{10}$$

3 Results

3.1 Performance evaluations of multiple DT-based ML models against FR model

The AUC value of ROC curve was higher for RF model (0.85) in comparison with the FR model (AUC = 0.72) DT model (AUC = 0.73), AdaBoost model (AUC = 0.74), GDBoost model (AUC = 0.83), XGBoost model (AUC = 0.84) (Fig. 5). Based on the ROC-AUC curve, it can be concluded that all the DT-based models have performed better than the FR model.

This study also determined the optimal ML model through the construction of confusion matrix and the assessment of multiple evaluation metrics including K-Fold cross validation, overall accuracy, precision score, recall score and F1 score.

Utilizing the confusion matrix with a sample of 60 testing data points reveals that RF model demonstrates the highest counts of True Positive (TP) of 24 and True negative (TN) of 24 (Fig. 6e). This model also achieved highest TPR of 82.75% with lowest FPR of 22.6% followed by AdaBoost with TPR (80.1%) and FPR (31.4%), DT with TPR (79.1%) and FPR (33.4%), XGBoost with TPR (78.5%) and FPR(28.1%), and lastly GdBoost with TPR (75.1%) and FPR (31.2%).

In the context of multiple evaluation metrics, RF emerged as a superior model in comparison to others decision-tree based ML models (Fig. 7). For example, the analysis of K-fold cross validation (fivefold) reveals that RF achieved the highest mean score of 0.80 outperforming XGBoost (0.77), GdBoost (0.75), AdaBoost (0.73) and DT (0.71). Furthermore, RF consistently showed the highest accuracy values in other evaluation metrics including overall accuracy (0.80), precision score (0.77), recall score (0.82) and F1 score (0.80) (Fig. 7). Since RF model performed the best among all DT-based ML models, this study considered the results of RF model to be further compared with FR results.

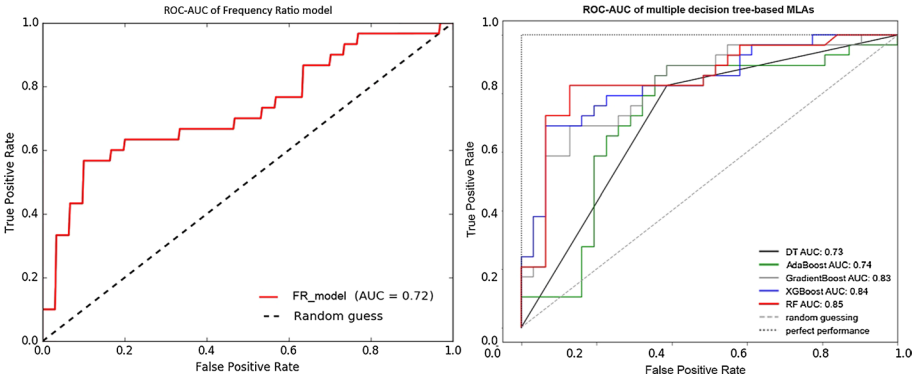

Fig. 5 ROC curve for FR and RF model. X axis represents false positive rate and Y axis represents true positive rate

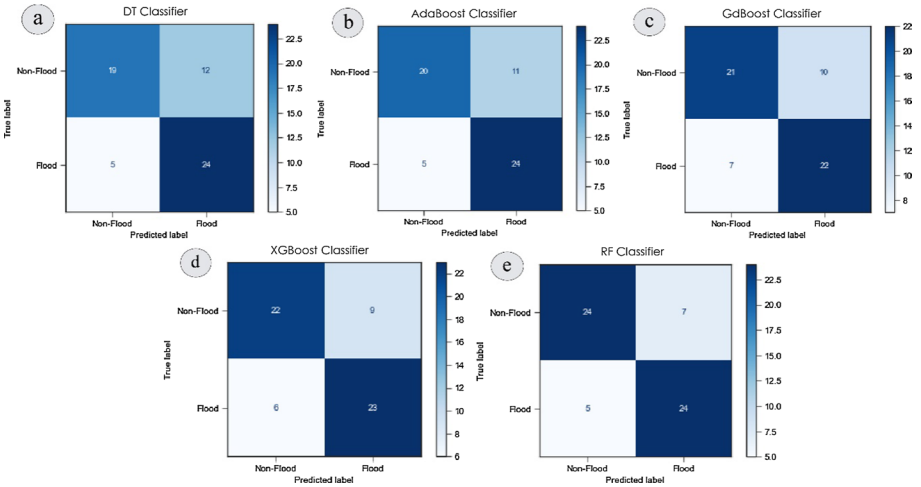

Fig. 6 Confusion matrix of multiple decision tree-based ML models

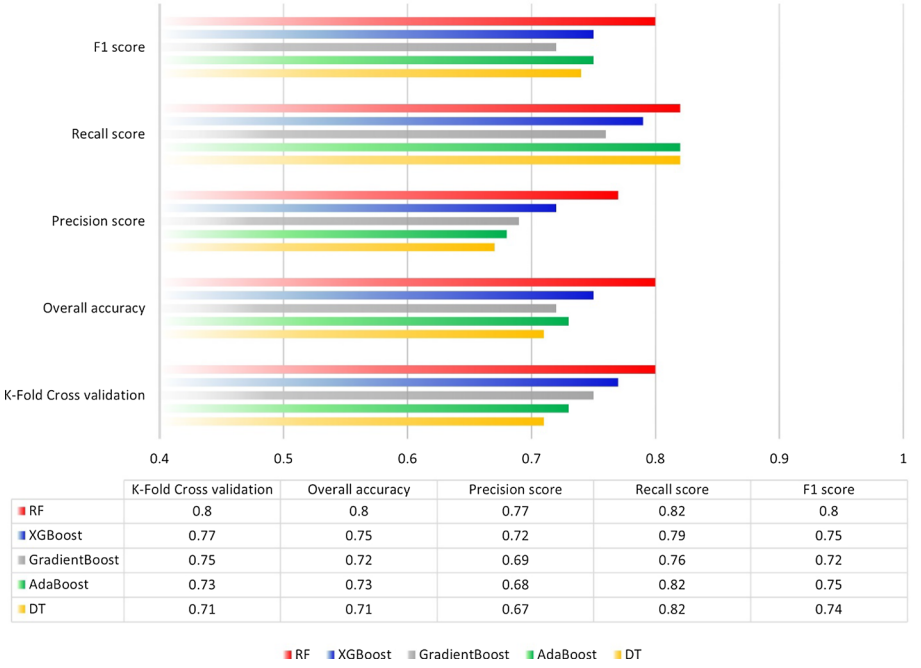

	K-Fold Cross validation	Overall accuracy	Precision score	Recall score	F1 score
RF	0.8	0.8	0.77	0.82	0.8
XGBoost	0.77	0.75	0.72	0.79	0.75
GradientBoost	0.75	0.72	0.69	0.76	0.72
AdaBoost	0.73	0.73	0.68	0.82	0.75
DT	0.71	0.71	0.67	0.82	0.74

Fig. 7 Accuracy assessment results of DT-based ML models from multiple evaluation metrics

3.2 Impact of each flood conditioning factor on flood occurrence

Figure 8 illustrates the impact of different FCFs on the occurrence of flooding. The findings from the RF model indicate that elevation has the highest impact (30.78%) on flooding

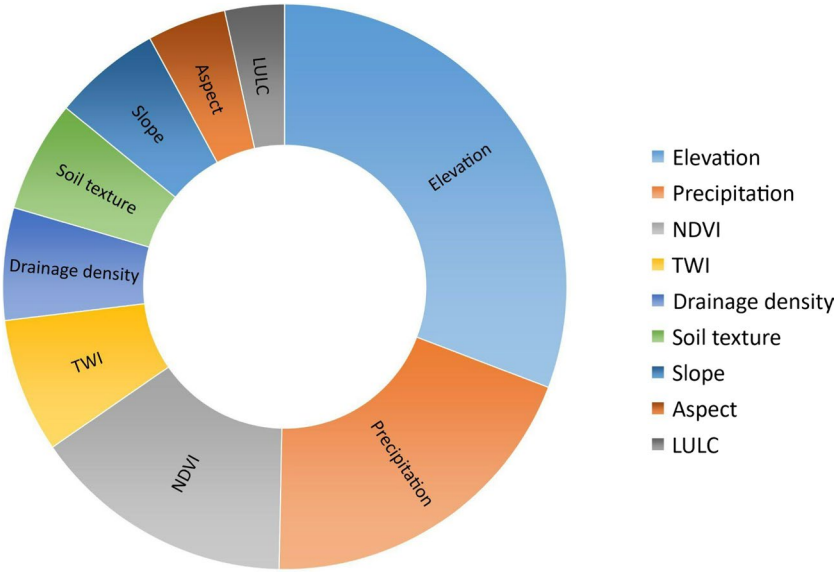

Fig. 8 Impact of flood conditioning factors on flooding in New Orleans

while precipitation has the second highest impact (19.53%) on the occurrence of floods in New Orleans. Furthermore, NDVI contributed 15.07%, TWI accounted for 7.69%, drainage density had 6.42% impact, soil texture affected by 6.38%, and slope had 6.17% impact on flood occurrence in New Orleans.

Moreover, LULC showed the lowest impact (3.43%), and aspect had the second lowest impact (4.51%) on flooding. Combined, elevation and precipitation accounted for 50.31% of the total flood susceptibility.

3.3 Comparison of results from the frequency ratio and random forest models

Overlaying various thematic layers of FCFs with the flood inventory map yields the FSMs from both the FR and RF models (Fig. 9). Depending on the flood susceptibility scores from the FR and RF models respectively, the entire city of New Orleans has been classified into five categories ranging from very low to very high. Overall, the eastern part of the city has higher flood susceptibility (in both models) compared to the western part, especially areas surrounding Lake Saint Catherine. In the urban area, several pockets have moderate flooding risks. In particular, neighborhoods to the north of the Mississippi River, such as part of the central business district (CBD), Audubon, uptown, and the Garden District, are faced with moderate to high flooding risks. Several neighborhoods to the east of the CBD, such as Bywater, St. Claude, and Holy Cross are at similarly elevated flood susceptibility. The Lower Ninth Ward, which has received wide attention in the aftermath of Hurricane Katrina, is currently at a low to moderate susceptibility of flooding in both models.

Based on the flood susceptibility results from the FR model, about 18.52% (114.51 km^2) of New Orleans city is classified as a very low susceptibility zone, 29.57% (182.79 km^2) as a low susceptibility zone, 25.94% (160.37km^2) as a moderate susceptibility zone, 17.46% (107.93 km^2) as a high susceptibility zone, and 8.51% (52.61 km^2) as a very high susceptibility zone (Table 4).

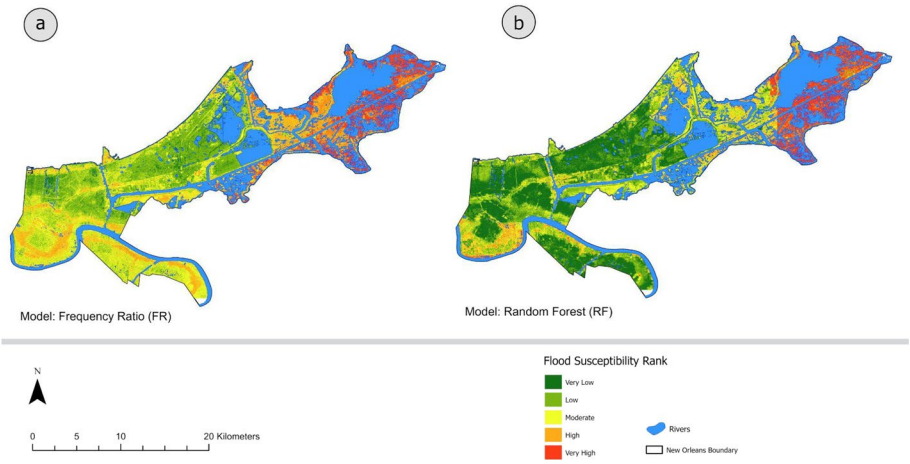

Fig. 9 The flood susceptibility maps of New Orleans city. **a** FSM produced by FR model. **b** FSM produced by RF model

Table 4 Spatial distribution of different flood susceptibility zones in New Orleans city

Susceptibility categories	FR		RF	
	Estimated susceptible area (km^2)	% Of area	Estimated susceptible area (km^2)	% Of area
Very low	114.51	18.52	199.24	32.23
Low	182.79	29.57	178.01	28.79
Moderate	160.37	25.94	116.45	18.84
High	107.93	17.46	67.12	10.86
Very high	52.61	8.51	57.37	9.28

The study also reveals that 34.64% of the total population in of New Orleans are area exposed to very high and high flood susceptible zones (25.97% areas of New Orleans) according to the FR model, while 23.21% of the total population are exposed to high and very high susceptible zones (20.14% of the total area), according to the RF model

In comparison, the RF model categorizes approximately 32.23% (199.24 km^2) of the New Orleans region as having a very low susceptibility, 28.79% (178.01 km^2) as low susceptibility, 18.84% (116.45 km^2) as moderate susceptibility, 10.86% (67.12 km^2) as high susceptibility, and 9.28% (57.37 km^2) as very high susceptibility (Table 4). The biggest differences of results generated by both models lie in the very low susceptibility (18.52% vs. 32.23%) and high susceptibility (17.46% vs. 10.86%). The FR model overestimated the high susceptibility area to be much larger, and very low susceptibility area substantially smaller, compared to the RF model.

4 Discussion

The discussion of this study covers two primary aspects. First, it compares the performance of FR model with that of DT based ML models in flood susceptibility assessment. Second, it discusses the primary contributing factors to flood occurrence and distribution of flood susceptibility zones in New Orleans.

The interactions between flood occurrence and FCFs are complex and non-linear. When dealing with complex and non-linear interactions between predictors and target variables, ML models surpass conventional statistical models in terms of accuracy (Goetz et al. 2015). To validate this assertion, this study compared the performances of multiple DT-based ML models with a statistical model (FR) using ROC AUC curve. Every DT-based ML model showed better classification performance compared to the FR model, as evidenced with higher AUC values (Fig. 5). This finding is consistent with previous studies that assessed different natural hazards susceptibilities. For instance, many researchers observed that the RF model outperformed the statistical models in landslide susceptibility assessment (Akinci and Zeybek 2021; Wang et al. 2020b), land subsidence and sinkholes susceptibility mapping (Elmahdy et al. 2020), seismic vulnerability assessment (Han et al. 2020), wildfire susceptibility mapping (Oliveira et al. 2012), groundwater potentiality mapping (Thanh et al. 2022) and debris flow susceptibility mapping (Liang et al. 2020).

The superior accuracy of DT-based ML models over the conventional FR model are likely due to a few facts. First, the straightforward formula of the statistical FR model oversimplifies the interactions between flood points and FCFs by neglecting non-flood points and solely depends on the total weight or class weights that makes this model prone to underfitting (Shahabi et al. 2020). Furthermore, most of the statistical models are based on the assumption of linearity, which is often violated by the relations between flood occurrence and various FCFs. These relationships have complex, dynamic and non-linear structures in nature. On the contrary, ML models can detect the existence of non-linear trends and can effectively handle non-linear relationships between any feature and the input variables (Oliveira et al. 2012; Tehrany et al. 2015b). Moreover, as our study shows, ML models take non-flood point into consideration along with flood point to ensure more balanced predictions. Second, standalone statistical models are less efficient in handling high dimensional large datasets (Amare et al. 2021). On the other hand, combining ML models into an ensemble can provide higher accuracies with large and high dimensional datasets than any standalone statistical models. Third, statistical models require data preprocessing and they are less efficient in dealing with multicollinearity issues among independent variables while ML models such as RF do not require any preprocessing and can effectively solve the multi-collinearity automatically (Liang et al. 2020).

While RF model shows the highest accuracy in ROC curve (AUC = 0.85), this study conducted a more comprehensive accuracy assessment employing various evaluation metrics to verify if the RF indeed stands out as the best model among all DT-based ML models. Through this comprehensive analysis of multiple evaluation metrics, it become evident that the RF model has emerged as the top performing ML model in flood susceptibility assessment (Figs. 6, 7). In the RF model, each tree divides the factors in pairs and then their predictions are aggregated, which makes each factor's contribution to prediction more independently. Consequently, even if some trees indicate dependent factors, others suppress them and yield the best results (Akinci and Zeybek 2021). Some other exceptional characteristics of the RF model, including proficiency of detecting the non-linear trends, insensitivity to noise, ability to reduce errors caused by missing data and outliers, ability to resolve multicollinearity, adaptability to both numerical or categorical data, make this model more robust and accurate

comparatively (Amare et al. 2021; Breiman 2001; Liang et al. 2020; Rodrigues and De la Riva 2014; Youssef et al. 2022). Taking all these findings and facts into account, the RF model can be deemed as the benchmark model for accurately mapping flood susceptibility at a local scale (Islam et al. 2021).

Furthermore, the RF model can rank each conditioning factor based on its contribution to flooding (Fig. 8). According to the results, low elevation and high precipitation in New Orleans contributed most to flooding. In southern Louisiana, and New Orleans in particular, small changes (of a meter or two) in elevation often mean the difference between being flooded or not. The region is deltaic, built from sediments from the Mississippi River. It is therefore relatively flat, low-lying, and some sections of the city are maintained within the levee protection system that are below mean sea level (MSL). The range in elevation runs from approximately 5.8 m above MSL to (-) 3.7 m below MSL (Campanella 2006). As such, these small variations in sea level largely determine which regions experience the highest frequency of flooding. Variations in precipitation were also found to explain a large proportion of the variance. This is likely related to the geographic precipitation pattern. The water bodies surrounding New Orleans promote a more stable atmosphere around the perimeter of New Orleans, while the urban environment promotes more rain towards the center of the city. This ultimately leads to higher flood susceptibility in some of the lower-lying locations within the city. The most populated area in this city is below sea level, rendering it highly vulnerable to flooding. Although a large levee system has been long constructed to provide residents protection from flooding, the levees have failed significantly numerous times in recent history, during Hurricane Betsy (1965), Camille (1969), and Katrina (2005) (Cass et al. 2023). Meanwhile, New Orleans has experienced an increasing number of heavy rainfall events (Brown et al. 2019; Keim and Muller 1992 and 1993; Powell and Keim 2015). Due to its major contribution to flood susceptibility, this unsettling increasing trend of extreme precipitation calls for special attention from planners and policy makers.

This study further used FR and RF models to generate FSMs of New Orleans and estimate exposed populations in areas with high flood susceptibility. Both models suggested that the eastern part of the city, particularly the areas surrounding Lake Saint Catherine, have higher susceptibility to flooding compared to the western part. The RF model classified a large portion of the western part as having very low susceptibility, whereas the FR model categorized them as low to moderate susceptibility, therefore, they disagreed in this case. The FR model exhibited a notable difference in estimation compared to RF model due to its low classification accuracy and oversimplified algorithmic approach. The FR model categorized 25.97% of areas as very high and high flood susceptible, where 34.64% of the total population resides, appears to be an overestimation. Conversely, the RF model delineated a more reasonable estimation of 20.14% areas as very high and high flood susceptible wherein 23.21% of the populations are the potential exposed.

5 Conclusion

Using New Orleans as a test bed, this study systematically compared the performance of statistical FR model with that of DT-based ML models in flood susceptibility mapping. Several key findings stand out from this research.

- DT-based ML models performed better than the conventional statistical FR model. This highlights their abilities to identify the nonlinear trends between flooding and FCFs effectively, which the FR model oversimplifies the relationships.
- A comprehensive performance evaluation using various metrics affirmed the RF model as the most accurate among the DT-based ML models for flood susceptibility mapping at a local scale.
- Several FCFs such as elevation and precipitation patterns were identified as the dominant contributors to flooding in New Orleans.
- Both RF and FR models indicate higher flood susceptibility in the eastern part of the city compared to the western part, but the FR model overestimated percentage of exposed populations (34.64%) in very high and high susceptible zone compared to RF model (23.21%).

Several implications can be drawn from this study. This study highlighted the importance of integrating ML models into the flood disaster risk reduction framework, especially at a local scale like New Orleans. Such integration of advanced ML models will not only contribute to increasing our knowledge about flood hazards but also inform future research in this area. It also provides actionable insights for policy makers and other practitioners by identifying significant factors of flooding such as low elevation and high precipitation in New Orleans. Moreover, the simulated FSM will serve as a valuable tool for the local disaster management authority throughout all phases of flood management including long-term mitigation, preparation, emergency response, and recovery. The use of ML models in urban flood susceptibility mapping can guide planners in future urban developments, by accurately identifying regions characterized as highly susceptible to flooding. By avoiding intense development of housing and infrastructure in the high-susceptible areas, immense economic losses can be prevented. The integration of ML models into the disaster risk reduction framework can also guide effective and equitable allocation of resources for disaster preparation and inform the development of disaster resilience infrastructure by prioritizing areas at heightened susceptibility. Policy makers can ensure the availability of flood-resistant infrastructure and emergency services in these highly susceptible regions to facilitate more efficient flood management strategies.

In the meantime, it is important to note that there are several limitations to this research. For instance, this study gathered flood inventory points solely from Sentinel-1 SAR dataset. As ML models are heavily dependent on the quality of the training data and any inaccuracies in the training data can produce misleading outcomes. Cross-examination of flood inventory points from multiple sources for training can be beneficial to ensure more reliable predictions. Furthermore, each geographic region has a unique set of FCFs. The primary contributing factors of flood susceptibility are likely different elsewhere. When moving to another area, FCFs that are unique to the local geography should be considered. Last, this study only considered physical geographical factors such as elevation and precipitation in flood susceptibility assessment. In order to assess flood risk, which is the outcome of the interaction of physical and social factors, social vulnerability needs to be considered. Future studies therefore should consider incorporating socioeconomic data for comprehensive flood risk assessment using more comprehensive target variables such as flood damages to train the models.

Funding Funding was provide by National Oceanic and Atmospheric Administration (Grant No. PO-0000182731).

Declarations

Conflict of interests The authors declare that they have no known competing financial interests or personal relationships that could have appeared to influence the work reported in this paper.

References

Abedi R, Costache R, Shafizadeh-Moghadam H, Pham QB (2022) Flash-flood susceptibility mapping based on XGBoost, random forest and boosted regression trees. Geocarto Int 37(19):5479–5496

Akinci H, Zeybek M (2021) Comparing classical statistic and machine learning models in landslide susceptibility mapping in Ardanuc (Artvin). Turk Nat Hazards 108(2):1515–1543

Al-Abadi AM (2018) Mapping flood susceptibility in an arid region of southern Iraq using ensemble machine learning classifiers: a comparative study. Arab J Geosci 11:1–19

Ali SA, Khatun R, Ahmad A, Ahmad SN (2019) Application of GIS-based analytic hierarchy process and frequency ratio model to flood vulnerable mapping and risk area estimation at Sundarban region. India Modeling Earth Syst Environ 5(3):1083–1102

Amare S, Langendoen E, Keesstra S, Ploeg MVD, Gelagay H, Lemma H, van der Zee SE (2021) Susceptibility to gully erosion: applying random forest (RF) and frequency ratio (FR) approaches to a small catchment in Ethiopia. Water 13(2):216

Ayalew L, Yamagishi H (2005) The application of GIS-based logistic regression for landslide susceptibility mapping in the Kakuda-Yahiko mountains central Japan. Geomorphology 65(1–2):15–31

Beven, J.L., Hagan, A., and Berg, R. (2022). Hurricane Ida 26 August – 1 September 2021. National Hurricane Center Tropical Cyclone Report, 163 pp. https://www.nhc.noaa.gov/data/tcr/AL092021_Ida.pdf

Breiman L (2001) Random forests. Mach Learn 45:5–32

Brown VM, Keim BD, Black A (2019) Climatology and trends in hourly precipitation for the Southeast United States. J Hydrometeorol 20(8):1737–1755

Campanella, R. (2006). Geographies of New Orleans: Urban Fabrics Before the Storm. Center for Louisiana Studies, University of Louisiana-Lafayette, Lafayette, Louisisana, 433 pp

Cai H, Lam N, Zou L, Qiang Y, Li K (2016) Assessing community resilience to coastal hazards in the lower Mississippi River Basin. Water 8(2):46–64

Cass E, Shao W, Hao F, Moradkhani H, Yeates E (2023) Identifying trends in interpretation and responses to hurricane and climate change communication tools. Int J Disaster Risk Reduct. https://doi.org/10.1016/j.ijdrr.2023.103752

Costache R, Pham QB, Avand M, Linh NTT, Vojtek M, Vojteková J, Dung TD (2020) Novel hybrid models between bivariate statistics, artificial neural networks and boosting algorithms for flood susceptibility assessment. J Environ Manag 265:110485

Dano UL, Balogun AL, Matori AN, Wan Yusouf K, Abubakar IR, Said Mohamed MA, Pradhan B (2019) Flood susceptibility mapping using GIS-based analytic network process: a case study of Perlis Malaysia. Water 11(3):615

Das S (2020) Flood susceptibility mapping of the Western Ghat coastal belt using multi-source geospatial data and analytical hierarchy process (AHP). Remote Sens Appl: Soc Environ 20:100379

Elkhrachy I, Pham QB, Costache R, Mohajane M, Rahman KU, Shahabi H, Anh DT (2021) Sentinel-1 remote sensing data and hydrologic engineering centres river analysis system two-dimensional integration for flash flood detection and modelling in New Cairo City Egypt. J Flood Risk Manag 14(2):e12692

Elliott J, Pais J (2006) Race, class, and Hurricane Katrina: Social differences in human responses to disaster. Soc Sci Res 35(2):295–321

Elmahdy SI, Mohamed MM, Ali TA, Abdalla JED, Abouleish M (2020) Land subsidence and sinkholes susceptibility mapping and analysis using random forest and frequency ratio models in Al Ain UAE. Geocarto Int 37(1):315–331

Falah, F., Rahmati, O., Rostami, M., Ahmadisharaf, E., Daliakopoulos, I. N., & Pourghasemi, H. R. (2019). Artificial neural networks for flood susceptibility mapping in data-scarce urban areas. In *Spatial modeling in GIS and R for Earth and Environmental Sciences* (pp. 323–336). Elsevier.

Farhadi H, Najafzadeh M (2021) Flood risk mapping by remote sensing data and random forest technique. Water 13(21):3115

FEMA (2006) Hurricane Katrina in the Gulf Coast (FEMA 548). Federal Emergency Management Agency, Washington DC

Finch C, Emrich CT, Cutter SL (2010) Disaster disparities and differential recovery in new Orleans. Popul Environ 31:179–202

Géron, A. (2022). *Hands-on machine learning with Scikit-Learn, Keras, and TensorFlow*. " O'Reilly Media, Inc.".
Ghanim AA, Shaf A, Ali T, Zafar M, Al-Areeq AM, Alyami SH, Rahman S (2023) An improved flood susceptibility assessment in Jeddah, Saudi Arabia, using advanced machine learning techniques. Water 15(14):2511
Goetz JN, Brenning A, Petschko H, Leopold P (2015) Evaluating machine learning and statistical prediction techniques for landslide susceptibility modeling. Comput Geosci 81:1–11
Gorelick N, Hancher M, Dixon M, Ilyushchenko S, Thau D, Moore R (2017) Google earth engine: planetary-scale geospatial analysis for everyone. Remote Sens Environ 202:18–27
Hallegatte S, Green C, Nicholls RJ, Corfee-Morlot J (2013) Future flood losses in major coastal cities. Nat Clim Chang 3:802–806. https://doi.org/10.1038/nclimate1979
Han J, Kim J, Park S, Son S, Ryu M (2020) Seismic vulnerability assessment and mapping of Gyeongju, South Korea using frequency ratio, decision tree, and random forest. Sustainability 12(18):7787
Hasanuzzaman M, Islam A, Bera B, Shit PK (2022) A comparison of performance measures of three machine learning algorithms for flood susceptibility mapping of river Silabati (tropical river, India). Phys Chem Earth Parts a/b/c 127:103198
Held IM, Soden BJ (2006) Robust responses of the hydrological cycle to global warming. J Clim 19(21):5686–5699
Hengl T (2018). Soil texture classes (USDA system) for 6 soil depths (0, 10, 30, 60, 100 and 200 cm) at 250 m (Version v02) [Data set]. Zenodo. 10.5281/zenodo.1475451
Hoque MAA, Tasfia S, Ahmed N, Pradhan B (2019) Assessing spatial flood vulnerability at Kalapara Upazila in Bangladesh using an analytic hierarchy process. Sensors 19(6):1302
Islam ARMT, Talukdar S, Mahato S, Kundu S, Eibek KU, Pham QB, Linh NTT (2021) Flood susceptibility modelling using advanced ensemble machine learning models. Geosci Front 12(3):101075
Islam MM, Sado K (2000) Development of flood hazard maps of Bangladesh using NOAA-AVHRR images with GIS. Hydrol Sci J 45(3):337–355
Jenks GF (1967) The data model concept in statistical mapping. Int Yearb Cartogr 7:186–190
Keim, B. D., & Muller, R. A. (2009). *Hurricanes of the Gulf of Mexico*. LSU Press. 232 pp.
Keim BD, Muller RA (1993) Frequency of heavy rainfall events in New Orleans, Louisiana, 1900 to 1991. Southeast Geogr 33(2):159–171
Keim BD, Muller RA (1992) Magnitude Fluctuations of Heavy Rainfall in New Orleans, Louisiana: 1871–1991. Water Resour Bull 28(4):721–730
Khosravi K, Pham BT, Chapi K, Shirzadi A, Shahabi H, Revhaug I, Bui DT (2018) A comparative assessment of decision trees algorithms for flash flood susceptibility modeling at Haraz watershed, northern Iran. Sci Total Environ 627:744–755
Khosravi K, Pourghasemi HR, Chapi K, Bahri M (2016) Flash flood susceptibility analysis and its mapping using different bivariate models in Iran: a comparison between Shannon's entropy, statistical index, and weighting factor models. Environ Monit Assess 188:1–21
Kia MB, Pirasteh S, Pradhan B, Mahmud AR, Sulaiman WNA, Moradi A (2012) An artificial neural network model for flood simulation using GIS: Johor River Basin Malaysia. Environ Earth Sci 67(1):251–264
Kopp RE, DeConto RM, Bader DA, Hay CC, Horton RM, Kulp S, Oppenheimer M, Pollard D, Strauss BH (2017) Evolving understanding of Antarctic ice-sheet physics and ambiguity in probabilistic sea-level projections. Earth's Future 5:1217–1233. https://doi.org/10.1002/2017EF000663
Lee, M.-J., Kang, J.-e., & Jeon, S. (2012). *Application of frequency ratio model and validation for predictive flooded area susceptibility mapping using GIS.* Paper presented at the 2012 IEEE international geoscience and remote sensing symposium.
Lee S, Kim JC, Jung HS, Lee MJ, Lee S (2017) Spatial prediction of flood susceptibility using random-forest and boosted-tree models in Seoul metropolitan city, Korea. Geomat Nat Haz Risk 8(2):1185–1203
Liang Z, Wang CM, Zhang ZM, Khan KUJ (2020) A comparison of statistical and machine learning methods for debris flow susceptibility mapping. Stoch Env Res Risk Assess 34:1887–1907
Madhuri R, Sistla S, Srinivasa Raju K (2021) Application of machine learning algorithms for flood susceptibility assessment and risk management. J Water Clim Change 12(6):2608–2623
Manandhar, B. (2010). Flood plain analysis and risk assessment of Lothar Khola. *Master of Science Thesis in Watershed Management. Tribhuvan University Institute of Forestry Pokhara, Nepal*.
National Centers for Environmental Information. (2019). Assessing the U.S. Climate in 2019. https://www.ncei.noaa.gov/news/national-climate-201912

National Academies of Sciences, Engineering, and Medicine (2019). Framing the Challenge of Urban Flooding in the United States. Washington, DC: The National Academies Press. https://doi.org/10.17226/25381.
Ogden FL, Pradhan NR, Downer CW, Zahner JA (2011) Relative importance of impervious area, drainage density, width function, and subsurface storm drainage on flood runoff from an urbanized catchment. Water Resour Res 47:W12503. https://doi.org/10.1029/2011WR010550
Oliveira S, Oehler F, San-Miguel-Ayanz J, Camia A, Pereira JM (2012) Modeling spatial patterns of fire occurrence in Mediterranean Europe using multiple regression and random forest. For Ecol Manage 275:117–129
Omer, S (2021). 2021 Hurricane Ida: Facts, FAQs, and how to help. World Vision. https://www.worldvision.org/disaster-relief-news-stories/2021-hurricane-ida-facts (Accessed on February 28, 2022).
Paul GC, Saha S, Hembram TK (2019) Application of the GIS-based probabilistic models for mapping the flood susceptibility in Bansloi sub-basin of Ganga-Bhagirathi river and their comparison. Remote Sens Earth Syst Sci 2(2):120–146
Pedregosa F, Varoquaux G, Gramfort A, Michel V, Thirion B, Grisel O, Duchesnay É (2011) Scikit-learn: machine learning in python. J Mach Learn Res 12:2825–2830
Pekel JF, Cottam A, Gorelick N, Belward AS (2016) High-resolution mapping of global surface water and its long-term changes. Nature 540(7633):418–422
Pistrika AK, Jonkman SN (2010) Damage to residential buildings due to flooding of New Orleans after hurricane Katrina. Nat Hazards 54:413–434
Powell EJ, Keim BD (2015) Trends in Daily Temperature and Precipitation Extremes for the Southeastern United States: 1948–2012. J Climate 28:1592–1612. https://doi.org/10.1175/JCLI-D-14-00410.1
Quader MA, Dey H, Malak MA, Sajib AM (2021) Rohingya refugee flooding and changes of the physical and social landscape in Ukhiya, Bangladesh. Environ Dev Sustain 23:4634–4658
Rahman M, Ningsheng C, Islam MM, Dewan A, Iqbal J, Washakh RMA, Shufeng T (2019) Flood susceptibility assessment in Bangladesh using machine learning and multi-criteria decision analysis. Earth Syst Environ 3(3):585–601
Rahman M, Ningsheng C, Mahmud GI, Islam MM, Pourghasemi HR, Ahmad H, Dewan A (2021) Flooding and its relationship with land cover change, population growth, and road density. Geosci Front 12(6):101224
Rahmati O, Pourghasemi HR, Zeinivand H (2016) Flood susceptibility mapping using frequency ratio and weights-of-evidence models in the Golastan Province Iran. Geocarto Int 31(1):42–70
Rodrigues M, De la Riva J (2014) An insight into machine-learning algorithms to model human-caused wildfire occurrence. Environ Model Softw 57:192–201
Sahana M, Rehman S, Sajjad H, Hong H (2020) Exploring effectiveness of frequency ratio and support vector machine models in storm surge flood susceptibility assessment: a study of Sundarban biosphere reserve. India Catena 189:104450
Samanta RK, Bhunia GS, Shit PK, Pourghasemi HR (2018) Flood susceptibility mapping using geospatial frequency ratio technique: a case study of Subarnarekha River Basin India. Modeling Earth Syst Environ 4(1):395–408
Sarkar D, Mondal P (2020) Flood vulnerability mapping using frequency ratio (FR) model: a case study on Kulik river basin Indo-Bangladesh Barind Region. Appl Water Sci 10(1):1–13
Shahabi H, Shirzadi A, Ghaderi K, Omidvar E, Al-Ansari N, Clague JJ, Ahmad A (2020) Flood detection and susceptibility mapping using sentinel-1 remote sensing data and a machine learning approach: hybrid intelligence of bagging ensemble based on k-nearest neighbor classifier. Remote Sens 12(2):266
Shahabi H, Shirzadi A, Ronoud S, Asadi S, Pham BT, Mansouripour F, Bui DT (2021) Flash flood susceptibility mapping using a novel deep learning model based on deep belief network, back propagation and genetic algorithm. Geosci Front 12(3):101100
Sweet, W.V., B.D. Hamlington, R.E. Kopp, C.P. Weaver, P.L. Barnard, D. Bekaert, W. Brooks, M. Craghan, G. Dusek, T. Frederikse, G. Garner, A.S. Genz, J.P. Krasting, E. Larour, D. Marcy, J.J. Marra, J. Obeysekera, M. Osler, M. Pendleton, D. Roman, L. Schmied, W. Veatch, K.D. White, and C. Zuzak, (2022). Global and Regional Sea Level Rise Scenarios for the United States: Updated Mean Projections and Extreme Water Level Probabilities Along U.S. Coastlines. NOAA Technical Report NOS 01. National Oceanic and Atmospheric Administration, National Ocean Service, Silver Spring, MD, 111 pp. https://oceanservice.noaa.gov/hazards/sealevelrise/noaa-nostechrpt01- global-regional-SLR-scenarios-US.pdf
Tehrany MS, Pradhan B, Jebur MN (2013) Spatial prediction of flood susceptible areas using rule based decision tree (DT) and a novel ensemble bivariate and multivariate statistical models in GIS. J Hydrol 504:69–79
Tehrany MS, Lee MJ, Pradhan B, Jebur MN, Lee S (2014) Flood susceptibility mapping using integrated bivariate and multivariate statistical models. Environ Earth Sci 72(10):4001–4015

Tehrany MS, Pradhan B, Jebur MN (2015a) Flood susceptibility analysis and its verification using a novel ensemble support vector machine and frequency ratio method. Stoch Env Res Risk Assess 29:1149–1165

Tehrany MS, Pradhan B, Mansor S, Ahmad N (2015b) Flood susceptibility assessment using GIS-based support vector machine model with different kernel types. CATENA 125:91–101

Tehrany MS, Kumar L (2018) The application of a Dempster–Shafer-based evidential belief function in flood susceptibility mapping and comparison with frequency ratio and logistic regression methods. Environ Earth Sci 77(13):1–24

Tellman B, Sullivan JA, Kuhn C, Kettner AJ, Doyle CS, Brakenridge GR, Slayback DA (2021) Satellite imaging reveals increased proportion of population exposed to floods. Nature 596(7870):80–86

Thanh NN, Chotpantarat S, Trung NH, Ngu NH (2022) Mapping groundwater potential zones in Kanchanaburi Province, Thailand by integrating of analytic hierarchy process, frequency ratio, and random forest. Ecol Ind 145:109591

Tien Bui D, Ho TC, Pradhan B, Pham BT, Nhu VH, Revhaug I (2016) GIS-based modeling of rainfall-induced landslides using data mining-based functional trees classifier with AdaBoost, Bagging, and MultiBoost ensemble frameworks. Environ Earth Sci 75:1–22

Tripathi R, Sengupta SK, Patra A, Chang H, Jung IW (2014) Climate change, urban development, and community perception of an extreme flood: A case study of Vernonia, Oregon, USA. Appl Geogr 46:137–146

USGCRP (2018): Impacts, Risks, and Adaptation in the United States: Fourth National Climate Assessment, Volume II: [Reidmiller, D.R., C.W. Avery, D.R. Easterling, K.E. Kunkel, K.L.M. Lewis, T.K. Maycock, and B.C. Stewart (eds.)]. U.S. Global Change Research Program, Washington, DC, USA, 1515 pp. doi: https://doi.org/10.7930/NCA4.2018.

Wang Y, Fang Z, Hong H, Peng L (2020a) Flood susceptibility mapping using convolutional neural network frameworks. J Hydrol 582:124482

Wang Y, Sun D, Wen H, Zhang H, Zhang F (2020b) Comparison of random forest model and frequency ratio model for landslide susceptibility mapping (LSM) in Yunyang County (Chongqing, China). Int J Environ Res Public Health 17(12):4206

Wang Z, Liu Q, Liu Y (2020c) Mapping landslide susceptibility using machine learning algorithms and GIS: A case study in Shexian county, Anhui province China. Symmetry 12(12):1954

Wing OEJ, Lehman W, Bates PD et al (2022) Inequitable patterns of US flood risk in the Anthropocene. Nat Clim Chang. https://doi.org/10.1038/s41558-021-01265-6

Wong, P.P., Losada, I.J., Gattuso, J.-P., Hinkel, J., Khattabi, A., Mclnnes, K.L., Saito, Y., Sallenger, A., (2014). Coastal Systems and Low-lying Area (Retrieved from Cambridge, United Kingdom and New York, NY, USA).

Youssef AM, Pourghasemi HR, El-Haddad BA (2022) Advanced machine learning algorithms for flood susceptibility modeling—performance comparison: Red Sea. Egypt Environ Sci Pollut Res 29(44):66768–66792

Authors and Affiliations

Hemal Dey[1,4] · Wanyun Shao[1,2,4] · Hamid Moradkhani[2,3] · Barry D. Keim[5] · Brad G. Peter[6]

✉ Wanyun Shao
wshao1@ua.edu

[1] Department of Geography and the Environment, University of Alabama, Tuscaloosa, USA

[2] Center for Complex Hydrosystems Research, University of Alabama, Tuscaloosa, USA

[3] Department of Civil, Construction, and Environmental Engineering, University of Alabama, Tuscaloosa, USA

[4] Alabama Water Institute, University of Alabama, Tuscaloosa, USA

[5] Department of Geography and Anthropology, Louisiana State University, Baton Rouge, USA

[6] Department of Geosciences, University of Arkansas, Fayetteville, USA